Self-assembled nanostructures on metal surfaces and graphene

Schmidt, Nico Daniel Robert

6 Organic Charge-Transfer Complexes on Ag(111): Evolution of Common Unoccupied Molecular States

Over the past years, molecular layers consisting of electron donating and accepting molecules have attracted increasing attention due to their potential usage in optoelectronic devices. Key parameters for understanding and tuning their performance are intermolecular and molecule-substrate interactions. Here we report on the formation of a blend of organic donors and acceptors from 1,4,5,8,9,12-hexaazatriphenylene-hexacarbonitril (HATCN) and 2,3,6,7,10,11-hexakis-alkoxytriphenylene (HAT) on a Ag(111) surface. We used scanning tunneling microscopy and spectroscopy, valence and core level photoelectron spectroscopy, and low-energy electron diffraction measurements complemented by density functional theory calculations to investigate both the electronic and structural properties of the homomolecular as well as the intermixed layers. For a homomolecular layer of donor molecules, we found a weak interaction with the Ag(111) surface, while for the acceptor molecules a strong interaction with the substrate leading to charge transfer and substantial buckling of the top silver layer as well as of the adsorbates was determined. Upon mixing acceptor and donor molecules, hybridization between the two different molecules leading to the emergence of a common unoccupied molecular orbital located at both – donor and acceptor molecule – was found. The donor acceptor blend studied is therefore a compelling

candidate for organic electronics based on self-assembly of charge-transfer complexes.

6.1 Introduction

Organic molecules are considered highly valuable for applications ranging from organic light emitting diodes[1] over organic photovoltaics[2] to field effect transistors[3] and molecular sensors.[4] Already nowadays they are used as active material in a variety of devices due to their low costs, easy processabilitly, light weight, structural flexibility, and tunablity of their electronic properties by molecular synthesis.[5] However, the intermolecular interactions in those devices are often governed by rather weak van der Waals interactionslimiting the performance of today's devices.

In order to unravel the interplay of intermolecular and molecule-substrate interactions which play a key-role in the device performance, considerable fundamental research on homomolecular layers on different metal substrates has been performed in the last three decades.[6–9] In contrast, studies on the electronic and structural properties of bi-component systems have only emerged in the last few years.[10–12] Special focus has been put on the organic-inorganic and organic-organic interface, which determines key properties like contact resistance, charge injection and extraction.[7,13,14]

One approach for increasing intermolecular interactions is based on equipping the organic molecules with complementary functional groups, e.g. hydrogen-bond donating and accepting groups.[12,15–18] In the last few years, the use of fluorinated molecules in mixed molecular layers leading to hydrogen-fluorine bonds was studied intensely.[19–23] Besides the increased

intermolecular interaction of fluorinated molecule with hydrogen-bond donating molecules, the fluorination induces electron accepting character of the molecules.[24–29] Due to their halogen bonds, strong intermolecular interaction can be achieved. Consequently, the resulting intermixed layers often showed similar self-assembly patterns independent of the underlying metal substrate.[11]

One of the first examples where monolayer thick films of electronically strongly interacting mixtures of donor and acceptor molecules were investigated is the case of tetrathiafulvalene and tetracyanoquinodimethane (TTF/TNCQ).[30] These molecules are known to form a three-dimensional bulk charge-transfer salt exhibiting metallic properties with a conductivity of $1.47 \times 10^4\ \Omega^{-1}\ cm^{-1}$.[31] On an Au(111) surface it was reported that a dispersing quasi one-dimensional band along the TCNQ molecules exists. Its origins lie in a complex mixing of metal and molecular states giving rise to a new interface state, which cannot be explained by the electronic properties of the single molecular components.[30]

Recently also a number of other charge-transfer (CT) complexes – thin films as well as crystalline samples – were investigated by means of ultra-violet photoelectron spectroscopy (UPS), X-ray photoelectron spectroscopy (XPS), near-edge x-ray absorption fine structure (NEXAFS) measurements, and density functional theory (DFT) calculations.[32–35] In these studies, mostly evaporated or solution-processed samples exploring TCNQ as acceptor and pyrene derivatives as donor[32–34] or coronene derivatives for both acceptor and donor,[35] were investigated. For the coronene derivatives, shifting of the core level binding energy of the donor

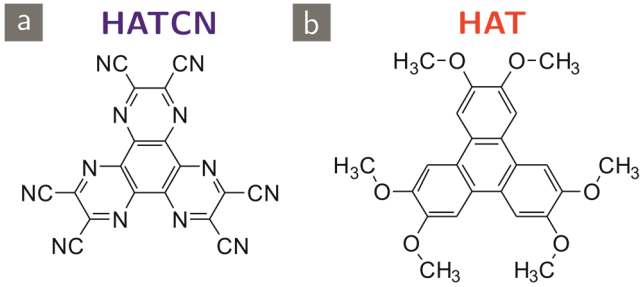

Scheme 6.1: Molecular structures: (a) HATCN (1,4,5,8,9,12-hexaazatriphenylene-hexacarbonitrile) and (b) HAT (2,3,6,7,10,11-hexakis-alkoxytriphenylene).

towards higher binding energy and of the acceptor towards lower binding energy were reported upon mixing, indicating a weak CT system.[35] In contrast, for the strong CT system of pyrene andTCNQ additional peaks were observed in the XPS and NEXAFS spectra indicating a hybridization of specific orbitals and ionization of the molecules due to charge-transfer.[32,33]

In this paper, we report on an organic donor/acceptor system from two complementary molecules, which exhibit threefold rotational symmetry and complementary electronic properties. As electron acceptor we used the well-known 1,4,5,8,9,12-hexaazatriphenylene-hexacarbonitrile (HATCN) molecule (Scheme 6.1a).[36,37] The organic electron donor used, 2,3,6,7,10,11-hexakis-alkoxytriphenylene (HAT) molecule (Scheme 6.1b), is known for its good electron donating properties when in contact with a strong acceptor.[38] The complementary character of the two molecules facilitated a well-ordered assembly in the mixed layer as observed by scanning tunneling microscopy (STM) and low-energy electron diffraction (LEED). Using scanning tunneling spectroscopy (STS), we identified a

common unoccupied state distributed across both molecules, which was not present for either of the homomolecular layers. These results point to a strong hybridization within the intermixed molecular layers. Our HATCN-HAT system thus represents a new strong candidate for organic (opto)electronic applications based on CT complexes.

6.2 Methods

Sample Preparation

All experiments were carried out under ultra-high vacuum (UHV) conditions. Ag(111) single crystals were cleaned by repeated cycles of Argon ion sputtering and subsequent annealing at 400 °C. The sample quality was checked by STM, XPS or LEED prior to molecule deposition. Molecules were deposited with a Knudsen cell evaporator and the evaporation rate was monitored by means of a quartz crystal microbalance. Typical evaporation rates were in the range of 0.2-0.5 ML/min, where one monolayer corresponds to full coverage of the surface with the (7x7) and $\left(\sqrt{21}\text{x}\sqrt{21}\right)R10.9°$ overlayer for HATCN and HAT, respectively. For the preparation of the intermixed structure, HAT molecules were deposited first followed by HATCN molecules. In order to improve the quality of the mixed layers for surface averaging measurements like XPS, ARPES and UPS, the samples were annealed at 150 °C after deposition of both molecules. The samples did not undergo any annealing for STM and STS measurements.

STM and STS Measurements

STM and STS measurements were performed in a two chamber UHV system equipped with a commercial low-temperature STM and a multi-channel plate (MCP) LEED optics (Scienta Omicron GmbH). STM images were either acquired at 77 K or at 5 K using a mechanically cut Pt/Ir tip. The bias voltages in the text are given with respect to a grounded tip. STS measurements were performed at 5 K with an external lock-in amplifier using a lock-in frequency of 678 Hz and a modulation voltage of 12 mV (rms-value) at liquid helium temperatures (5 K). WSxM was used to analyze the STM images.[39]

UPS and Work Function Measurements

UPS and work function measurements were carried out in a separate UHV system equipped with a variable temperature STM (Scienta Omicron GmbH), a hemispherical energy analyzer (Thermo Fisher), a twin anode X-ray source, a He discharge lamp, and LEED optics (SPECS). The STM was used to confirm that at least 90% of the surface was covered with molecules to ensure a reasonable intensity for spectroscopy measurements. For the measurements of the intermixed samples, at least 90% of the molecules were arranged in the above described mixed structure. The overall quality of the samples was determined with LEED. UPS was performed by using a non-monochromatized HeI lab source (21.2 eV) under an angle of approx. 30° with respect to the surface normal and with an acceptance angle of approx. 12°. Work function measurements were performed by applying a bias of -5 V to the sample and measuring the secondary electron cut-off and the Fermi level.

XPS and ARPES Measurements

XPS and angle-resolved photoelectron spectroscopy (ARPES) measurements were performed in a multi-chamber UHV system equipped with an analyzer chamber containing a SPECS 150 hemispherical analyzer. ARPES measurements were performed with monochromatized HeI radiation (21.2 eV) under an angle of 5° with respect to the surface normal in order to remove the intensity coming from the surface state of the Ag(111). In another chamber, a Kratos Axis Ultra XPS system containing a monochromatized Al K_α X-ray source was used to acquire high-resolution XPS data. The preparation chamber contained LEED optics (SPECS). However, the system did not contain a STM to monitor the structural quality of the samples. Hence, coverage and quality of the molecular films was investigated in different ways. First, the amount of molecules necessary for 1 ML of HAT could be estimated by LEED as the molecules were mobile at room temperature for coverages below 1 ML and only for coverages close to 1 ML a sharp LEED pattern could be observed. Secondly, the molecular coverage was determined by monitoring the silver surface state with ARPES, which was shifted into the unoccupied states for samples covered with a full monolayer of molecules. A weak remainder of the original silver surface state indicated that the surface was almost completely covered with molecules, without having a second molecular layer. Finally, the quality of the LEED pattern for the intermixed structure and absence of LEED spots related to pure HAT or HATCN domains was used to confirm that the majority of the sample was covered by the above-described intermixed phase.

The binding energy of the XPS data was referenced to the Ag $3d_{5/2}$ peak at 368.3 eV.[40] Subtraction of the silver plasmon peaks, which overlap with the N 1s region, was carried out in the following way: The N 1s background region was measured for one monolayer of HAT molecules, which do not contain any nitrogen.[41] This spectrum was smoothed, the intensities of all spectra were aligned at the low binding energy site of the region and then the background spectrum was subtracted from the data measured for HATCN and for the intermixed layer. For all spectra a Shirley-type background was subtracted except for the O 1s region where a linear background was employed. The peaks were fitted by a combination of Lorentzian and Gaussian functions. For the N 1s spectra, the area ratio of the two components was constrained to 1:1. The ARPES data were fitted by a simple Lorentzian function after subtraction of a linear background (see Appendix for more details).

6.3 Results and Discussion

Structural and Electronic Properties of HATCN and HAT

Before discussing the adsorption on Ag(111), the structural and electronic properties of HAT and HATCN in the gas phase are briefly described. Our DFT calculations show that both molecular backbones are planar in the gas phase. Furthermore, the HAT molecule can exist in different conformations due to the rotational flexibility of the O-CH_3 groups. The most stable conformation is shown in Scheme 6.1b.

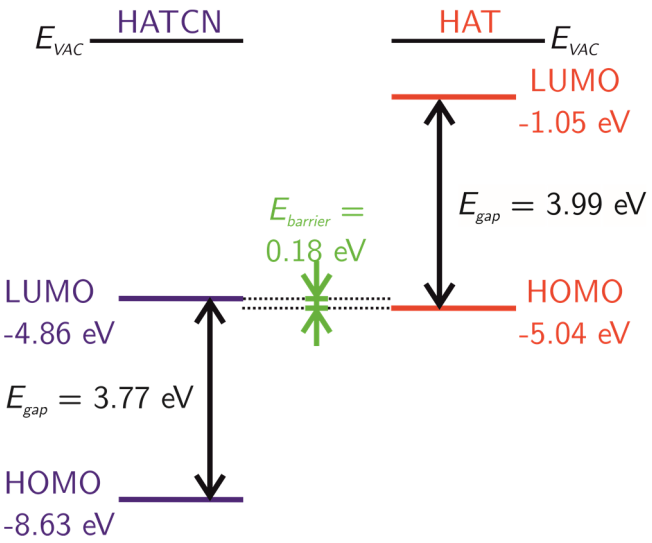

Fig. 6.1: Energy levels of HATCN (left) and HAT (right) determined by DFT calculations.

In Fig. 6.1 the energy diagrams of the two molecules derived from DFT calculations of the gas phase molecules are shown. The highest occupied molecular orbital (HOMO) of the HAT molecule is found 5.04 eV below the vacuum level while the lowest unoccupied molecular orbital (LUMO) of HATCN resides 4.86 eV below the vacuum level. This leads to a charge injection barrier of only 0.18 eV for a charge transfer from the HOMO of HAT into the LUMO of HATCN. These values compare rather well with energy values derived from optical and electrochemical measurements,[42,43] although the experimentally deduced charge injection barrier is higher (1.1 eV) (Appendix Fig. A6.1). Nonetheless, both DFT calculation and measured energy levels highlight the electronic complementarity of HATCN and HAT and their excellent suitability to form CT complexes.

Self-Assembly of the Molecules

In the following, we describe the self-assembly of the homomolecular layers as well as the blend of HATCN and HAT on the Ag(111) surface. For coverages ≤ 1 monolayer (ML), HATCN molecules formed a porous hexagonal network. In the close-up STM image presented in Fig. 6.2a the triangular shape arising from the hexaazatriphenylene-backbone of the molecules is clearly visible. As known from literature, the cyano groups generally cannot be imaged in STM.[44,45] The long-range order was interrupted by dislocation lines and stacking faults (Fig. A6.2a). No mirror or rotational domains were observed in the STM images. The LEED pattern (Fig. 6.2a, middle column) displays a (7x7) superstructure, which is in line with the absence of rotational domains. Combining the information from LEED and STM and using the lattice constant of Ag (4.09 Å), the unit cell can be described by $a = b = 2.02$ nm and an enclosing angle of $\theta = 120°$. The tentative structure model (Fig. 6.2a, right column), which was derived from the STM and LEED observations, demonstrates that the molecular network is stabilized by dipolar coupling between the negatively charged N-atoms and the positively charged C-atoms of neighboring cyano groups. Our DFT calculations showed a similar self-assembled arrangement with a molecule-molecule distance of 1.2 nm (Fig. A6.9a and b). The adsorption energy is 2.41 eV/molecule and the average adsorption height of the carbon atoms is 2.99 Å (Table A6.3). Furthermore, the DFT calculations indicate that the cyano groups are significantly bent towards the substrate leading to a strong buckling of the

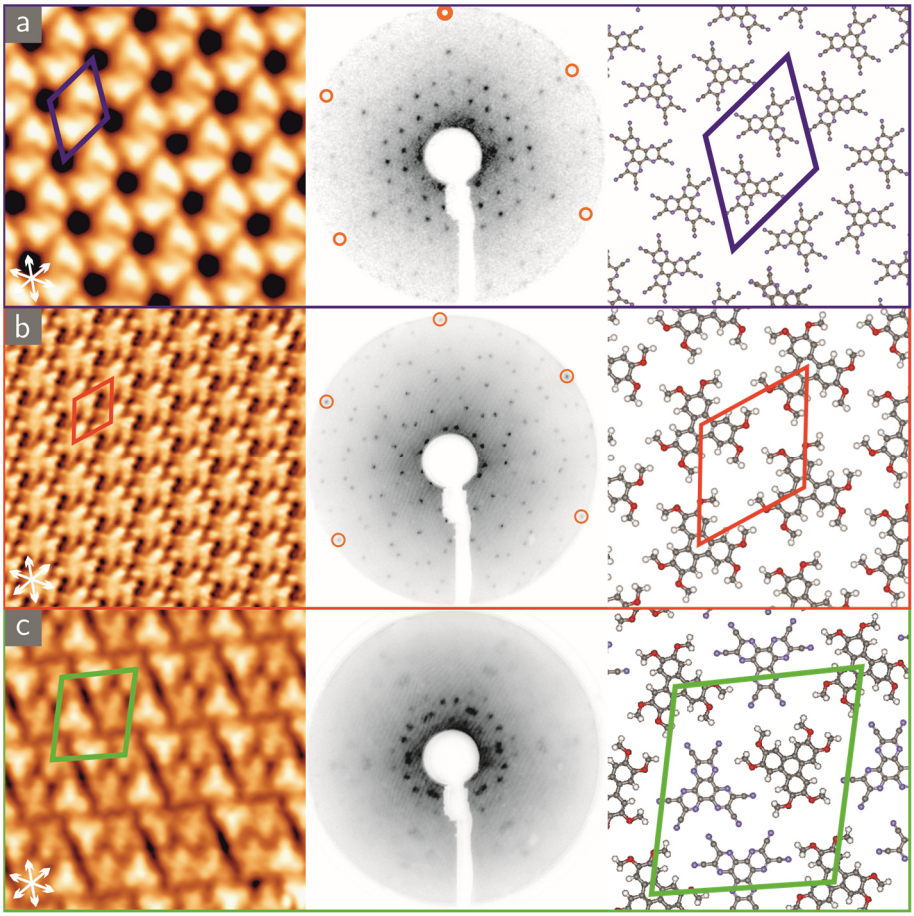

Fig. 6.2 Self-assembly of (a) HATCN, (b) HAT, and (c) HAT+HATCN on Ag(111). The substrate orientation is indicated by white arrows in the STM images. STM parameters: (a) T = 77 K, U = 0.5 V, I = 150 pA, 8 x 8 nm^2; (b) T = 77 K, U = 0.2 V, I = 30 pA, 8 x 8 nm^2; (c) T = 77 K, U = 0.5 V, I = 40 pA, 8 x 8 nm^2. Middle column: LEED patterns taken at 36 eV (a), 37 eV (b) and 15 eV (c); in (a) and (b) the substrate spots are indicated by orange circles. Right column: tentative structure models; the unit cells are indicated in blue, red, and green for (a), (b) and (c), respectively.

molecule as well as of the top surface layer. Our findings for HATCN on Ag(111) are in line with those reported by Glowatzki et al.[46]

For coverages ≤ 1 ML, HAT molecules assembled into a hexagonal close-packed network as depicted in Fig. 6.2b. In the STM images, individual molecules appeared with six protrusions at their periphery. These "legs" derive from the six methoxy groups of the molecule. From the mirror-symmetric shape of the molecules it can be inferred that the molecules were adsorbed in the most stable configuration shown in Scheme 6.1b. For room temperature measurements, HAT was found to be mobile and the aforementioned network could only be observed for monolayer coverages. However, when measuring at 77 K HAT formed several hundred nanometer big islands of close-packed molecules with only a few vacancies (Fig. A6.2b). Sometimes, also one-dimensional molecular wires were observed. This was especially the case for low coverages as shown in Fig. A6.3 in the appendix. From the LEED pattern (Fig. 6.2b, middle column) a $\left(\sqrt{21}\mathrm{x}\sqrt{21}\right)R10.9°$ superstructure for HAT on Ag(111) can be determined which can be also described by a $\begin{pmatrix} 5 & 1 \\ -1 & 4 \end{pmatrix}$ matrix. Thus, two mirror domains rotated by $\pm 10.9°$ with respect to the Ag [1-10] direction were present on the surface (see white arrows in Fig. 6.2 for the substrate direction). The unit cell vectors of this network – derived from the LEED data – are $a = b = 1.32$ nm with an enclosing angle of $\theta = 120°$. The tentative structure model in Fig. 6.2b, right column shows one of the mirror domains. It is apparent that the molecular assembly is stabilized by hydrogen bonding between the H-atoms of the methyl groups and neighboring oxygen atoms. This self-assembly pattern is in agreement with

our DFT calculations, which showed a similar molecular orientation (Fig. A6.9c and d). In the simulated STM image the oxymethyl groups appear bright which is in line with our STM images. Our DFT calculations give an adsorption energy of HAT of 2.27 eV/molecule and show that the molecular backbone of HAT is adsorbed rather flat on the surface with an average adsorption height of the C-atoms of 3.34 Å (Table A6.4).

To facilitate successful intermixing of both molecules on the silver surface, HAT molecules were deposited first. Due to their high mobility at room temperature for sub-monolayer coverage, they could easily mix with the added HATCN molecules. After depositing an approximate one-to-one ratio of HAT and HATCN on Ag(111), a close-packed network was formed as shown in Fig. 6.2c. In large-scale STM images a row like pattern can be observed (Fig. A6.2c). The close-up view shown in Fig. 6.2c clearly indicates two differently appearing molecules. The brighter molecules exhibit a triangular shape while the dark molecules have an asymmetric cross-like shape. The bright, triangular molecules could be identified as the HATCN molecules as they showed the same appearance as in the pure HATCN layer (Fig. 6.2a). In contrast, the darker, asymmetric molecules do not exhibit the six symmetrically arranged "legs" observed for the pure HAT layer. The reason for this different appearance lies in the rotational flexibility of the oxymethyl groups of HAT, leading to several possible conformations. The most stable conformation shown in Scheme 6.1b was found for the homomolecular layer. In the conformation present in the bi-molecular layer, two of the methyl groups are rotated towards the neighboring oxymethyl groups while for one of the phenyl rings both methyl

legs are oriented to the outside. This specific conformation, which is shown in Scheme A6.1b in the appendix, leads to an asymmetric cross-like appearance seen in the STM image. Note that this conformation is energetically less favorable than the one observed in the homomolecular layer. The LEED pattern (Fig. 6.2c, middle column) is more complex than for the homomolecular assemblies. We propose that the intermixed molecular layer formed an incommensurate superstructure, since there is no integer matrix, which can describe the observed LEED pattern. Thus, the lengths of the unit cell vectors were only determined from STM data and measure $a = 2.4 \pm 0.1$ nm and $b = 2.7 \pm 0.1$ nm with an enclosing angle of $\theta = 103 \pm 3°$.[47] The observed adsorption pattern gives rise to six rotational domains on the surface. In the tentative structure model (Fig. 6.2c, right column) most cyano groups of a HATCN molecule form H-bonds with neighboring HAT molecules, while one cyano group undergoes dipolar coupling with another HATCN molecule. The dipolar coupling interaction is similar to the one observed for homomolecular HATCN structures. The unit cell contains two HATCN and two HAT molecules as indicated by the green tetragon in the tentative structure model (Fig. 6.2c, right column).

X-ray Photoelectron Spectroscopy

Fig. 6.3 shows XPS data for the N 1s and O 1s core levels taken on the homomolecular as well as the intermixed layers. Due to the many chemically different carbon species present in the two molecules, the C 1s spectra show a very complex behavior (Fig. A6.7). The N 1s spectrum of HATCN shows two components, which were fitted with a 1:1 area ratio.

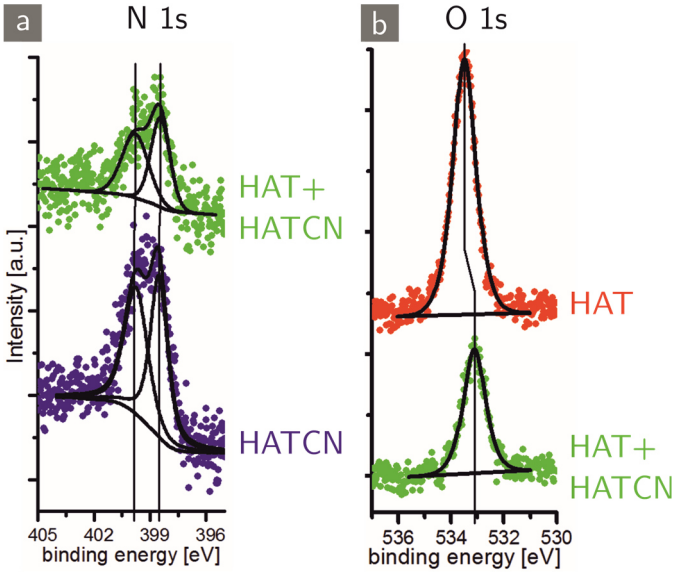

Fig. 6.3: XPS spectra for monolayers of HATCN (blue), HAT+HATCN (green) and HAT (red) (a) N 1s spectra, (b) O 1s spectra.

The peak at lower binding energy stems from the cyano component of HATCN while the peak at higher binding energy corresponds to the N-atoms in the heterocycle.[48] The O 1s spectra consist of only one component, which is in line with the chemical structure of the HAT molecule (Scheme 6.1b). For the intermixed molecular layer, the binding energies of the N 1s peaks of HATCN show almost no shifts. In contrast, the O 1s peak of HAT shifted by 0.4 eV towards lower binding energies when mixing with the acceptor molecule HATCN. A similar shift of the donor core levels to lower binding energy when mixing the donor with the acceptor molecule was shown in earlier reports.[11,21,24,35]

Electronic Properties

In a next step, we investigated the electronic properties of the homomolecular as well as the intermixed layers by means of ARPES, UPS and STS. The ARPES results for monolayer coverage of HATCN are shown in Fig. 6.4a. The blue line represents the angle-integrated intensity as function of the binding energy. A slight increase of the intensity close to the Fermi level was observed. This was also seen by angle-integrated UPS (Fig. A6.5b and d). We associate the increased intensity around the Fermi level with a partial filling of the LUMO of HATCN, which was also reported in an earlier publication.[46] This partial filling is in line with the Bader charge analysis of our DFT calculations, which showed a charge transfer of 2.3 electrons per molecule from the substrate into the molecule (Fig. A6.10). The HOMO of the pure HATCN could not be observed. The band gap of HATCN in gas phase was reported to be larger than 3 eV (Fig. 6.1).[43] We therefore suspect an overlapping of the HATCN HOMO with the silver 4d bands, which gave rise to a high intensity below -2.8 eV.

For approximately one monolayer of HAT, a clear band was found at -2.2 eV (Fig. 6.4b, red line), which can be associated with the HOMO of the HAT molecule. The HOMO calculated by DFT lies significantly higher in energy at -1.1 eV (Fig. A6.10). However, it is well known that the band gap of organic molecules is underestimated by DFT leading to this discrepancy in the calculated and measured DOS.[49]

In the case of the intermixed molecular layer, the HOMO was observed at -2.0 eV (Fig. 6.4c). We propose that this was the HAT HOMO shifted by approximately 0.2 eV towards the Fermi level when compared

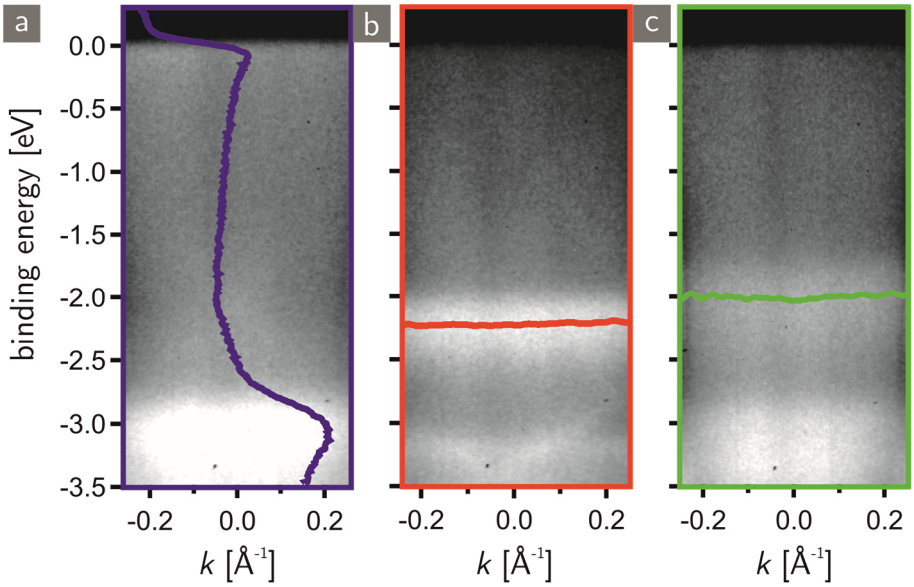

Fig. 6.4: ARPES data taken 5° off-normal emission for (a) HATCN, (b) HAT and (c) HAT+HATCN. The blue line in a) represents the angle integrated intensity as a function of the energy. The red and green line in b) and c) indicate the position of the HOMO derived from fits (Fig. A6.6) in the pure and in the intermixed layer, respectively. The high intensity around 3 eV arises from the Ag 4d bands.

to the homomolecular layer. A similar shift of the donor HOMO level towards the Fermi level for mixing of a donor with an acceptor molecule was also reported earlier.[21,50] Additionally, the HOMO of the intermixed layer was significantly broadened compared to the one of the pure HAT layer (Fig. A6.6). We relate this to a stronger interaction of the HAT molecule either with HATCN or with the metallic substrate.[51] In contrast, El-Sayed et al. reported a broader HOMO of the acceptor molecule in the homomolecular layer while its width was decreased in the intermixed molecular layer.[51] Furthermore, the increased intensity around the Fermi level observed for HATCN alone was significantly reduced in the intermixed

Table 6.1: Work function changes relative to the clean Ag(111) substrate measured by UPS and from DFT calculations.

	HATCN	HAT	HAT+HATCN
work function changes [eV] from UPS	0.0	-0.9	-0.4
work function changes [eV] from DFT	+0.1	-0.9	-

molecular layer (Fig. A6.5b and d). This demonstrates that the charge transfer between the substrate and HATCN was reduced upon deposition of the electron donating molecule (HAT) indicating a reduced HATCN-substrate interaction.

In addition to the ARPES results, we measured work function changes of the homo- and intermixed molecular layers, which are summarized in Table 6.1 and in Fig. A6.5c in the appendix. UPS measurements and DFT calculations showed that the work function of the HATCN monolayer on Ag(111) is similar to the one of the clean substrate. In contrast, the work function strongly decreased by 0.9 eV upon adsorption of a HAT monolayer on Ag(111). The work function of the intermixed layer resides between those of the homomolecular layers. Generally, the work function of a substrate decreases upon adsorption of organic molecules due to Pauli repulsion between the metal electron cloud and the electrons from the adsorbates. This effect can explain the reduction of the work function observed for monolayer coverage of HAT. For the monolayer of HATCN, the Pauli repulsion is counteracted by the charge transfer from the substrate to the HATCN molecules, leading to a surface dipole as observed by ARPES/UPS measurements and DFT calculations.

Our DFT calculations even showed a slight increase of the work function by 0.1 eV compared to the one of clean Ag(111). It should be noted that the work functions we determined by UPS are slightly higher (5.1 eV for both Ag(111) and HATCN on Ag(111)) than those reported in literature.[52] Nevertheless, the trend that the work function of flat-laying HATCN molecules on the Ag(111) surface is the same as for the clean Ag(111) is in line with earlier reports.[52]

Our observations of the work function changes can be well described by a method used by Goiri et al.[11] and El-Sayed et al.[21] For weakly interacting, bi-molecular systems the work function change of an intermixed molecular layer can be determined by the work function changes of the pure components as long as the surface areas occupied by the adsorbates are known. By deriving the surface area values from the unit cell parameters, we calculated a theoretical work function change of -0.43 eV (Eq. A1). This value is very close to the measured value of -0.4 eV showing that according to this method our system behaves like earlier reported donor/acceptor systems. [11,22]

In order to investigate the electronic properties on a local scale, STS was performed for the homomolecular and the intermixed phases. The results are summarized in Fig. 6.5. We focused on the unoccupied electronic states since the HOMO positions could be derived from the ARPES and UPS data. STS for the homomolecular HATCN layer shows that the surface state of Ag(111) is shifted above the Fermi level by around 90 meV with respect to the clean Ag(111) surface state (Fig. 6.5, dark blue line). Additionally, a small feature 70 mV below the Fermi level is

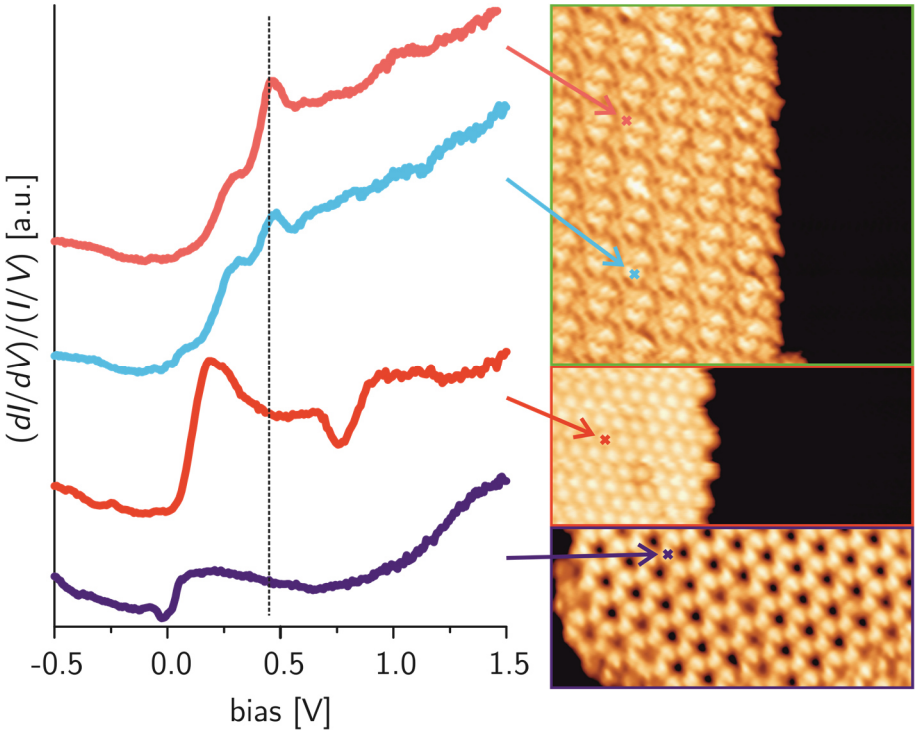

Fig. 6.5: STS data for the homomolecular HATCN and HAT islands (dark blue and red curve, respectively) and for the HATCN (light blue) as well as HAT (light red) molecule in the intermixed layer acquired at 5 K. The thin black line at 0.45 V indicates the position at which the dI/dV map in Fig. 6.6 was taken. The panel on the right shows the corresponding STM images. The colored crosses indicate at which positions the dI/dV spectra were taken. (Bottom right: HATCN 22 x 10 nm^2; center right: HAT 15.6 x 6.7 nm^2; top right: intermixed island 20 x 20 nm^2; set-point: U = -0.5 V, I = 200 pA for pure HAT and pure HATCN, U = +0.5 V, I = 200 pA for the intermixed island).

visible in the spectrum. We ascribe this to partial charge transfer from the Ag surface into the molecule, in line with our ARPES and work function measurements.[53] No further features were found in the STS spectra for the HATCN molecules within the investigated energy range.

For the homomolecular layer of HAT, a similar shift of the surface state into the unoccupied states was observed (Fig. 6.5, red line). Besides the shift of the surface state, a dip around 0.75 V in the density of states was found. We assume that the LUMO resides just below this dip around 0.65 V where a small increase in the density of states is visible. This is in line with our theoretical calculations where a small feature in the carbon pz orbitals is observed around 0.3 eV (Fig. A6.10). Keeping in mind that the band gap is usually underestimated by DFT, the LUMO is expected to lie at higher energies than the calculated one.[49]

When probing the electronic properties of the molecules in the intermixed layer, clear differences were observed. Qualitatively, there is no difference between the STS spectra acquired either on top of HAT molecules or on top of HATCN molecules (Fig. 6.5, two top most spectra). Both exhibited an increase in the density of states around 0.2 eV. The clear peak at around 0.45 eV can be assigned to an unoccupied molecular orbital (dotted black line). Note that neither HAT nor HATCN in the monomolecular layers showed a similar feature. In order to determine the local distribution of this unoccupied molecular orbital, dI/dV maps were taken at 0.45 eV for the intermixed phase. It is clearly visible that the cross-like HAT molecules in the intermixed layer appear brighter; i.e. they exhibit a higher conductivity than the triangular HATCN molecules (Fig. 6.6). This was also visible in the dI/dV spectra where the peak at 0.45 eV showed more intensity on top of the HAT molecule than on top of the HATCN molecule (Fig. 6.5 and Fig. A6.8). Interestingly, HAT molecules at the boarder of the intermixed island, which are not in contact with

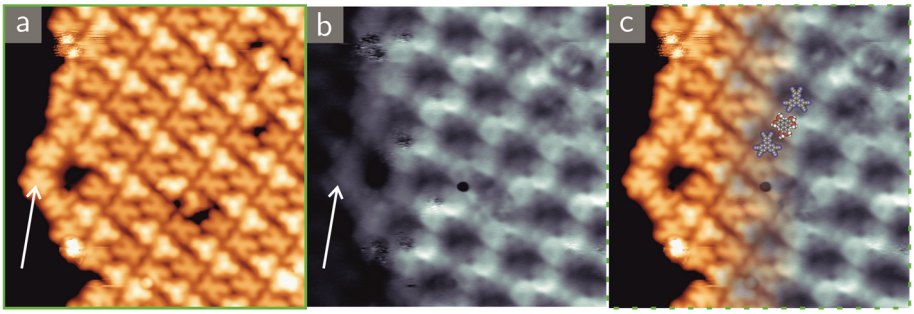

Fig. 6.6: STM image and simultaneously acquired dI/dV map of the intermixed layers taken at a bias of 0.45 V as indicated by the vertical line in Fig. 6.5, acquired at 5 K. (a) topography, (b) dI/dV map. (c) Superposition of the topography and the dI/dV map (12 x 12 nm^2, I = 200 pA). The white arrows in (a,b) point to a row of HAT molecules at the boarder of the island, which exhibit lower conductivity.

HATCN molecules (Fig. 6.6, white arrows) and exhibit the six-leg structure (Scheme 6.1b), showed a reduced conductivity compared to the molecules within the intermixed structure. This is a further indication that the electronic structure of HAT is changed upon mixing of the two molecules. Note that at the boarders of the intermixed islands the conductivity is the same as in the center of the island (Fig. A6.4). Thus, we exclude a spill-out effect, which might have induced this weaker contrast for the HAT molecules at the island borders. From the STS data we conclude that the two molecules hybridized in the intermixed layer leading to an alignment of the unoccupied molecular orbitals. This is in contrast to weakly interacting organic donor/acceptor systems like the combination of CuPc and F_{16}CuPc on graphite were shifts of the HOMO and LUMO positions have been observed but no common molecular orbitals for both donor and acceptor molecules were reported.[50]

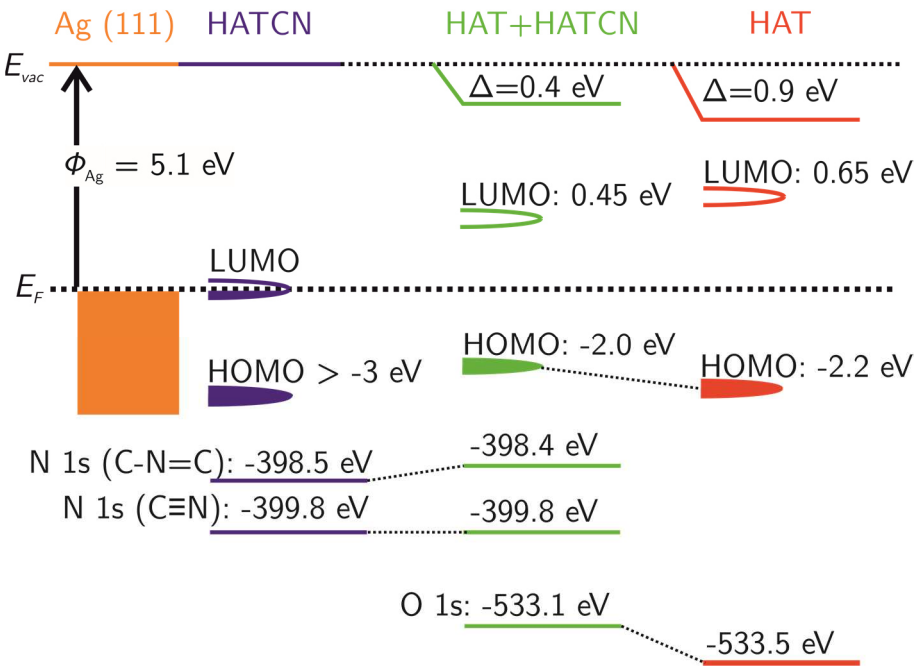

Fig. 6.7: Energy levels for HATCN and HAT and the intermixed phase on Ag(111), as derived from XPS, ARPES/UPS, and STS measurements.

Discussion

Fig. 6.7 depicts the energy levels of the homomolecular layers of the acceptor HATCN and the donor HAT and compares them to the energy levels of the intermixed molecular layer. The energy values were derived from ARPES/UPS, STS, and XPS measurements and are displayed with respect to the Fermi level. For weakly interacting organic donor/acceptor systems, a rigid shift away from the vacuum level was usually reported when increasing the amount of donor/acceptor ratio.[11,21,26] This was described by the so-called vacuum level pinning (VLP) model where all energies (conduction band, valence band and core levels) are pinned to the vacuum level.[11,21] In other words: if the work function is

reduced all energy levels will be shifted to lower values by a similar amount. This seems to be the case for the HAT molecule. The work function compared to the intermixed layer is reduced by 0.5 eV and the HOMO as well as the O 1s core level were shifted away from the Fermi level, although the shift of the HOMO only amounted to approximately half of the shift of the vacuum level and the O 1s binding energy. In the case of HATCN one might expect a Fermi level pinning (FLP) instead of a VLP.[21] This means that the work function decrease caused by the mixing of the two molecules was counteracted by a small charge redistribution of the partially filled LUMO at the Fermi level leaving the energy levels of the HATCN unaffected. Indeed, we observed a decreased intensity close to the Fermi level in the mixed layer compared to the pure HAT (Fig. A6.5d). However, the N 1s core levels did not show any significant changes in binding energy for the homomolecular and mixed layer, which is an indication for FLP.

However, the simple picture of the VLP model or the FLP model does not explain the hybridization of the donor and acceptor molecules leading to the alignment of the unoccupied molecular orbitals as observed in the STS measurements (Fig. 6.5). First of all the LUMO of HAT compared to the intermixed layer shifted toward E_{vac} by 0.2 eV while all other states showed a shift in the opposite direction. Secondly, our STS data showed that the electronic structure of the unoccupied states of both HAT and HATCN in the intermixed layer was similar. For both molecules a LUMO peak at 0.45 V was detected, which was neither for the homomolecular HAT nor for the homomolecular HATCN layer observed.

Our combined ARPES and DFT data show that HATCN exhibited a significant interaction with the Ag(111) surface in the homomolecular layer. In contrast, the structural and electronic properties of HAT were essentially unaffected upon adsorption on the Ag(111), as shown by our DFT calculations for gas phase and adsorbed HAT molecules in the homomolecular layer (see appendix). Intermixing HATCN and HAT led to a hybridization between the two molecules evidenced in the emergence of the new and common LUMO, which shows a spatially homogeneous distribution across both molecules. The hybridization was accompanied by a conformational change of HAT as can be seen from the STM data. We suspect that in the mixed layer the intermolecular interactions are considerable stronger than the molecule/substrate interaction, because the assemblies changed from commensurate in the homomolecular layers to incommensurate in the mixed layer. The increased intermolecular interaction was also manifested in the increased half-width of the HOMO of the HAT molecule (Fig. A6.6). Furthermore, we observed a reduce HATCN-substrate interaction in the mixed layer which resulted in a decreased FWHM of the N 1s peaks in the mixed layer and in a reduced charge transfer from the substrate into the HATCN (Fig. A6.5d and Table A6.2).

6.4 Conclusion

In conclusion, we studied two structurally and electronically complementary molecules on Ag(111). Both molecules assembled into well-ordered, commensurate structures for monolayer deposition. The electron donor HAT showed weak interaction with the Ag(111) surface, while for

the electron acceptor HATCN buckling and charge transfer into the LUMO were observed upon adsorption. By intermixing the two molecules, we found a strong hybridization leading to the emergence of a new and common unoccupied state not present for the homomolecular layers. Spatial mapping of this unoccupied state showed a homogeneous distribution across both molecules. Additionally, we have evidences that the intermolecular interaction is strongly increased in the mixed layer while the HATCN-substrate interaction is significantly reduced. Our HATCN+HAT system therefore represents a strong CT complex suitable for possible usage in organic (opto)electronics.

6.5 References

1. Reineke, S., Lindner, F., Schwartz, G., Seidler, N., Walzer, K., Lüssem, B. and Leo, K. (2009). White Organic Light-Emitting Diodes with Fluorescent Tube Efficiency. *Nature* **459**, 234–238
2. Fukuzumi, S. and Kojima, T. (2008). Photofunctional Nanomaterials Composed of Multiporphyrins and Carbon-Based π-Electron Acceptors. *Journal of Materials Chemistry* **18**, 1427–1439
3. Horowitz, G. (1998). Organic Field-Effect Transistors. *Advanced Materials* **10**, 365–377
4. Lin, P. and Yan, F. (2012). Organic Thin-Film Transistors for Chemical and Biological Sensing. *Advanced Materials* **24**, 34–51
5. Kagan, C. R., Mitzi, D. B. and Dimitrakopoulos, C. D. (1999). Organic-Inorganic Hybrid Materials as Semiconducting Channels in Thin-Film Field-Effect Transistors. *Science* **286**, 945–947
6. Otero, R., Vázquez de Parga, A. L. and Gallego, J. M. (2017). Electronic, Structural and Chemical Effects of Charge-Transfer at Organic/Inorganic Interfaces. *Surface Science Reports* **72**, 105–145
7. Ishii, H., Sugiyama, K., Ito, E. and Seki, K. (1999). Energy Level Alignment and Interfacial Electronic Structures at Organic Metal and Organic Organic Interfaces. *Advanced Materials* **11**, 605–625
8. Liang, H., He, Y., Ye, Y., Xu, X., Cheng, F., Sun, W., Shao, X., Wang, Y., Li, J. and Wu, K. (2009). Two-Dimensional Molecular Porous Networks Constructed by Surface Assembling. *Coordination Chemistry Reviews* **253**, 2959–2979
9. Koepf, M., Chérioux, F., Wytko, J. A. and Weiss, J. (2012). 1D and 3D Surface-Assisted Self-Organization. *Coordination Chemistry Reviews* **256**, 2872–2892
10. Zhang, J. L., Zhong, S., Zhong, J. Q., Niu, T. C., Hu, W. P., Wee, A. T. S. and Chen, W. (2015). Rational Design of Two-Dimensional Molecular Donor-Acceptor Nanostructure Arrays. *Nanoscale* **7**, 4306–4324
11. Goiri, E., Borghetti, P., El-Sayed, A., Ortega, J. E. and De Oteyza, D. G. (2016). Multi-Component Organic Layers on Metal Substrates. *Advanced Materials* **28**, 1340–1368
12. Bouju, X., Mattioli, C., Franc, G., Pujol, A. and Gourdon, A. (2017). Bicomponent Supramolecular Architectures at the Vacuum-Solid Interface. *Chemical Reviews* **117**, 1407–1444
13. Marmont, P., Battaglini, N., Lang, P., Horowitz, G., Hwang, J., Kahn, A., Amato, C. and Calas, P. (2008). Improving Charge Injection in Organic

Thin-Film Transistors with Thiol-Based Self-Assembled Monolayers. *Organic Electronics* **9**, 419–424

14. Braun, S., Salaneck, W. R. and Fahlman, M. (2009). Energy-Level Alignment at Organic/Metal and Organic/Organic Interfaces. *Advanced Materials* **21**, 1450–1472
15. Theobald, J. A., Oxtoby, N. S., Phillips, M. A., Champness, N. R. and Beton, P. H. (2003). Controlling Molecular Deposition and Layer Structure with Supramolecular Surface Assemblies. *Nature* **424**, 1029–1031
16. Whitesides, G. M., Simanek, E. E., Mathias, J. P., Seto, C. T., Chin, D. N., Mammen, M. and Gordon, D. M. (1995). Noncovalent Synthesis: Using Physical-Organic Chemistry to Make Aggregates. *Accounts of Chemical Research* **28**, 37–44
17. Llanes-Pallas, A., Matena, M., Jung, T., Prato, M., Stöhr, M. and Bonifazi, D. (2008). Trimodular Engineering of Linear Supramolecular Miniatures on Ag(111) Surfaces Controlled by Complementary Triple Hydrogen Bonds. *Angewandte Chemie - International Edition* **47**, 7726–7730
18. Gonzalez-Lakunza, N., Cañas-Ventura, M. E., Ruffieux, P., Rieger, R., Müllen, K., Fasel, R. and Arnau, A. (2009). Hydrogen-Bonding Fingerprints in Electronic States of Two-Dimensional Supramolecular Assemblies. *ChemPhysChem* **10**, 2943–2946
19. De Oteyza, D. G., Garcia-Lastra, J. M., Goiri, E., El-Sayed, A., Wakayama, Y. and Ortega, J. E. (2014). Asymmetric Response Toward Molecular Fluorination in Binary Copper-Phthalocyanine/Pentacene Assemblies. *Journal of Physical Chemistry C* **118**, 18626–18630
20. Barrena, E., De Oteyza, D. G., Dosch, H. and Wakayama, Y. (2007). 2D Supramolecular Self-Assembly of Binary Organic Monolayers. *ChemPhysChem* **8**, 1915–1918
21. El-Sayed, A., Borghetti, P., Goiri, E., Rogero, C., Floreano, L., Lovat, G., Mowbray, D. J., Cabellos, J. L., Wakayama, Y., Rubio, A., Ortega, J. E. and De Oteyza, D. G. (2013). Understanding Energy-Level Alignment in Donor-Acceptor/Metal Interfaces from Core-Level Shifts. *ACS Nano* **7**, 6914–6920
22. Goiri, E., Matena, M., El-Sayed, A., Lobo-Checa, J., Borghetti, P., Rogero, C., Detlefs, B., Duvernay, J., Ortega, J. E. and De Oteyza, D. G. (2014). Self-Assembly of Bicomponent Molecular Monolayers: Adsorption Height Changes and Their Consequences. *Physical Review Letters* **112**, 117602
23. Huang, Y. L., Chen, W., Li, H., Jing, M., Pflaum, J. and Wee, A. T. S. (2010). Tunable Two-Dimensional Binary Molecular Networks. *Small* **6**, 70–75

24. Wakayama, Y., De Oteyza, D. G., Garcia-Lastra, J. M. and Mowbray, D. J. (2011). Solid-State Reactions in Binary Molecular Assemblies of F16CuPc and Pentacene. *ACS Nano* **5**, 581–589
25. Borghetti, P., El-Sayed, A., Goiri, E., Rogero, C., Lobo-Checa, J., Floreano, L., Ortega, J. E. and De Oteyza, D. G. (2014). Spectroscopic Fingerprints of Work-Function-Controlled Phthalocyanine Charging on Metal Surfaces. *ACS Nano* **8**, 12786–12795
26. Borghetti, P., De Oteyza, D. G., Rogero, C., Goiri, E., Verdini, A., Cossaro, A., Floreano, L. and Ortega, J. E. (2016). Molecular-Level Realignment in Donor-Acceptor Bilayer Blends on Metals. *Journal of Physical Chemistry C* **120**, 5997–6005
27. Cabellos, J. L., Mowbray, D. J., Goiri, E., El-Sayed, A., Floreano, L., De Oteyza, D. G., Rogero, C., Ortega, J. E. and Rubio, A. (2012). Understanding Charge Transfer in Donor-Acceptor/Metal Systems: A Combined Theoretical and Experimental Study. *Journal of Physical Chemistry C* **116**, 17991–18001
28. De Oteyza, D. G., García-Lastra, J. M., Corso, M., Doyle, B. P., Floreano, L., Morgante, A., Wakayama, Y., Rubio, A. and Ortega, J. E. (2009). Customized Electronic Coupling in Self-Assembled Donor-Acceptor Nanostructures. *Advanced Functional Materials* **19**, 3567–3573
29. De Oteyza, D. C., Silanes, I., Ruiz-Osés, M., Barrena, E., Doyle, B. P., Arnau, A., Dosch, H., Wakayama, Y. and Ortega, J. E. (2009). Balancing Intermodular and Molecule-Substrate Interactions in Supramolecular Assemblies. *Advanced Functional Materials* **19**, 259–264
30. Gonzalez-Lakunza, N., Fernández-Torrente, I., Franke, K. J., Lorente, N., Arnau, A. and Pascual, J. I. (2008). Formation of Dispersive Hybrid Bands at an Organic-Metal Interface. *Physical Review Letters* **100**, 156805
31. Ferraris, J., Cowan, D. O., Walatka, V. and Perlstein, J. H. (1973). Electron Transfer in a New Highly Conducting Donor-Acceptor Complex. *Journal of the American Chemical Society* **95**, 948–949
32. Medjanik, K., Chercka, D., Nagel, P., Merz, M., Schuppler, S., Baumgarten, M., Müllen, K., Nepijko, S. A., Elmers, H. J., Schönhense, G., Jeschke, H. O. and Valenti, R. (2012). Orbital-Resolved Partial Charge Transfer from the Methoxy Groups of Substituted Pyrenes in Complexes with Tetracyanoquinodimethane - A Nexafs Study. *Journal of the American Chemical Society* **134**, 4694–4699
33. Medjanik, K., Gloskovskii, A., Kutnyakhov, D., Felser, C., Chercka, D., Baumgarten, M., Müllen, K. and Schönhense, G. (2012). Charge Transfer in the Novel Donor-Acceptor Complexes Tetra- and Hexamethoxypyrene with Tetracyanoquinodimethane Studied by HAXPES. *Journal of Electron Spectroscopy and Related Phenomena* **185**, 77–84

34. Medjanik, K., Perkert, S., Naghavi, S., Rudloff, M., Solovyeva, V., Chercka, D., Huth, M., Nepijko, S. A., Methfessel, T., Felser, C., Baumgarten, M., Müllen, K., Elmers, H. J. and Schönhense, G. (2010). Formation of an Intermolecular Charge-Transfer Compound in UHV Codeposited Tetramethoxypyrene and Tetracyanoquinodimethane. *Physical Review B - Condensed Matter and Materials Physics* **82**, 245419

35. Medjanik, K., Kutnyakhov, D., Nepijko, S. A., Schönhense, G., Naghavi, S., Alijani, V., Felser, C., Koch, N., Rieger, R., Baumgarten, M. and Müllen, K. (2010). Electronic Structure of Large Disc-Type Donors and Acceptors. *Physical Chemistry Chemical Physics* **12**, 7184–7193

36. Kurpil, B., Savateev, A., Papaefthimiou, V., Zafeiratos, S., Heil, T., Özenler, S., Dontsova, D. and Antonietti, M. (2017). Hexaazatriphenylene Doped Carbon Nitrides—Biomimetic Photocatalyst with Superior Oxidation Power. *Applied Catalysis B: Environmental* **217**, 622–628

37. Lemaur, V., Da Silva Filho, D. A., Coropceanu, V., Lehmann, M., Geerts, Y., Piris, J., Debije, M. G., Van De Craats, A. M., Senthilkumar, K., Siebbeles, L. D. A., Warman, J. M., Brédas, J. L. and Cornil, J. (2004). Charge Transport Properties in Discotic Liquid Crystals: A Quantum-Chemical Insight into Structure-Property Relationships. *Journal of the American Chemical Society* **126**, 3271–3279

38. Park, L. Y., Hamilton, D. G., McGehee, E. A. and McMenimen, K. A. (2003). Complementary C3-Symmetric Donor - Acceptor Components: Cocrystal Structure and Control of Mesophase Stability. *Journal of the American Chemical Society* **125**, 10586–10590

39. Horcas, I., Fernández, R., Gómez-Rodríguez, J. M., Colchero, J., Gómez-Herrero, J. and Baro, A. M. (2007). WSXM: A Software for Scanning Probe Microscopy and a Tool for Nanotechnology. *Review of Scientific Instruments* **78**, 013705

40. Moulder, J. F. (Perkin-Elmer Corporation, 1992). *Handbook of X-ray Photoelectron Spectroscopy: A Reference Book of Standard Spectra for Identification and Interpretation of XPS Data*.

41. A surface covered with one monolayer of molecules was used as reference instead of the clean silver surface, in order to account for the quenching of the silver Plasmon by the adsorbed molecules.

42. Schubert, M., Franzmann, P., Wünsche Von Leupoldt, A., Koszinowski, K., Heinze, K. and Waldvogel, S. R. (2016). Over-Oxidation as the Key Step in the Mechanism of the MoCl5-Mediated Dehydrogenative Coupling of Arenes. *Angewandte Chemie - International Edition* **55**, 1156–1159

43. Falkenberg, C., Olthof, S., Rieger, R., Baumgarten, M., Muellen, K., Leo, K. and Riede, M. (2011). The Role of Energy Level Matching in Organic

Solar Cells- Hexaazatriphenylene Hexacarbonitrile as Transparent Electron Transport Material. *Solar Energy Materials and Solar Cells* **95**, 927–932

44. Gottardi, S., Müller, K., Moreno-Lõpez, J. C., Yildirim, H., Meinhardt, U., Kivala, M., Kara, A. and Stöhr, M. (2014). Cyano-Functionalized Triarylamines on Au(111): Competing Intermolecular Versus Molecule/Substrate Interactions. *Advanced Materials Interfaces* **1**, 1–10
45. Müller, K., Moreno-Lõpez, J. C., Gottardi, S., Meinhardt, U., Yildirim, H., Kara, A., Kivala, M. and Stöhr, M. (2016). Cyano-Functionalized Triarylamines on Coinage Metal Surfaces: Interplay of Intermolecular and Molecule-Substrate Interactions. *Chemistry - A European Journal* **22**, 581–589
46. Glowatzki, H., Bröker, B., Blum, R. P., Hofmann, O. T., Vollmer, A., Rieger, R., Mullen, K., Zojer, E., Rabe, J. P. and Koch, N. (2008). 'Soft' Metallic Contact to Isolated C60 Molecules. *Nano Letters* **8**, 3825–3829
47. The unit cell parameters of the pure HATCN and HAT phases were determined from the commensurate superstructures found in LEED, while for the unit cell of the intermixed layer STM images were used. Consequently, the latter one exhibits some errors.
48. Christodoulou, C., Giannakopoulos, A., Nardi, M. V., Ligorio, G., Oehzelt, M., Chen, L., Pasquali, L., Timpel, M., Giglia, A., Nannarone, S., Norman, P., Linares, M., Parvez, K., Müllen, K., Beljonne, D. and Koch, N. (2014). Tuning the Work Function of Graphene-On-Quartz with a High Weight Molecular Acceptor. *Journal of Physical Chemistry C* **118**, 4784–4790
49. Ruiz-Osés, M., De Oteyza, D. G., Fernández-Torrente, I., Gonzalez-Lakunza, N., Schmidt-Weber, P. M., Kampen, T., Hom, K., Gourdon, A., Arnau, A. and Ortega, J. E. (2009). Non-Covalent Interactions in Supramolecular Assemblies Investigated with Electron Spectroscopies. *ChemPhysChem* **10**, 896–900
50. Zhong, J. Q., Qin, X., Zhang, J. L., Kera, S., Ueno, N., Wee, A. T. S., Yang, J. and Chen, W. (2014). Energy Level Realignment in Weakly Interacting Donor–Acceptor Binary Molecular Networks. *ACS Nano* **8**, 1699–1707
51. El-Sayed, A., Mowbray, D. J., García-Lastra, J. M., Rogero, C., Goiri, E., Borghetti, P., Turak, A., Doyle, B. P., Dell'Angela, M., Floreano, L., Wakayama, Y., Rubio, A., Ortega, J. E. and De Oteyza, D. G. (2012). Supramolecular Environment-Dependent Electronic Properties of Metal–Organic Interfaces. *Journal of Physical Chemistry C* **116**, 4780–4785
52. Niederhausen, J., Amsalem, P., Frisch, J., Wilke, A., Vollmer, A., Rieger, R., Müllen, K., Rabe, J. P. and Koch, N. (2011). Tuning Hole-Injection Barriers at Organic/Metal Interfaces Exploiting the Orientation of a

Molecular Acceptor Interlayer. *Physical Review B - Condensed Matter and Materials Physics* **84**, 165302

53. We can exclude that the dip at the Fermi level is due to a Kondo effect since the same feature was also observed for STS measurements at 77 K and it would be expected that the Kondo resonance is strongly reduced at higher temperatures.

6.6 Appendix

Different Conformations of HAT

Scheme A6.1 shows possible conformations of HAT, besides the one shown in Scheme 6.1b. Our gas phase calculations showed that conformation 2 (Scheme A6.1a) is 0.82 eV less stable compared to conformation 1 shown in the main text. Thus, rotation of the oxymethyl groups consumes energy. The conformation shown in Scheme A6.1bis the one, which we assign to the molecule conformation in the intermixed molecular structure.

Electrochemical Results

Fig. A6.1 shows the energy diagram derived from current-voltage (CV) curves and from literature.[42,43] While the data of HAT agree rather well with the calculated energy levels shown in Fig. 6.1 in the main text, the LUMO and HOMO of HATCN are shifted towards the vacuum level compared to the theoretical calculations. This results in a slightly higher charge injection barrier compared to the one calculated with DFT.

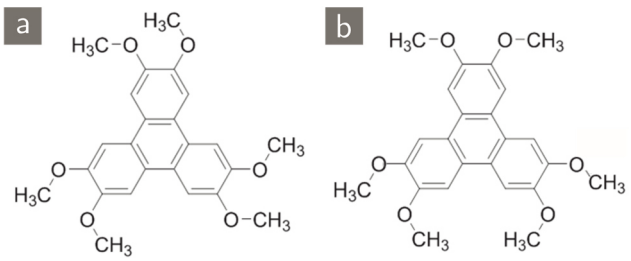

Scheme A6.1: Different conformations of the HAT molecule: (a) conformation 2; (b) conformation which was observed in the intermixed molecular layer.

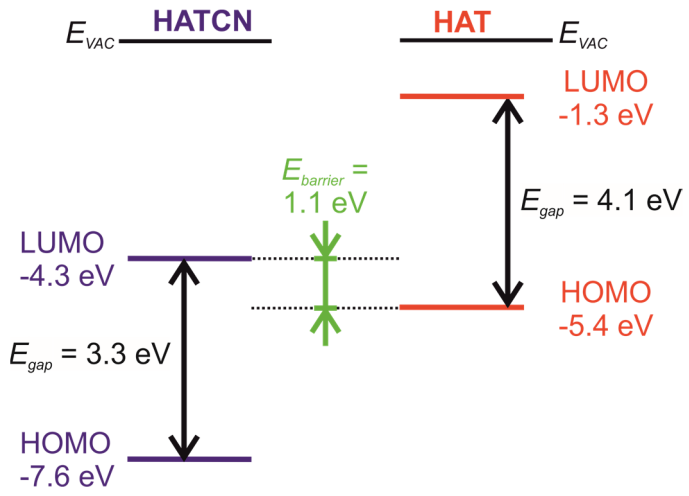

Fig. A6.1: Energy levels of HATCN (left) and HAT (right). The values for the HAT molecules are taken from reference [42]. The LUMO of HATCN was derived from CV-curves and the optical band gap was taken from reference [43].

Additional STM Images

Fig. A6.2 shows large scale STM images of HATCN (a), HAT (b), and the intermixed molecular layer (c). HACTN molecules formed a porous hexagonal network with a considerable amount of dislocation lines. In contrast, the HAT molecules formed islands of several hundreds of nm with only a few molecular vacancies visible. For the intermixed molecular layer different rotational domains were present on the surface (Fig. A6.2).

Besides the hexagonal close packed islands of HAT, sometimes 1D molecular chains were observed as well. An overview and a close-up STM image of theses chains also exhibiting branching are shown in Fig. A6.3

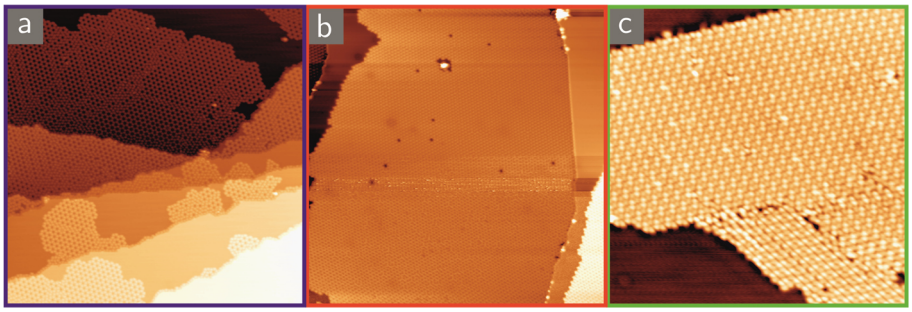

Fig. A6.2: Overview STM images. (a) HATCN (T = 77 K, U = 1.0 V, I = 120 pA, 100 x 100 nm^2), (b) HAT (T = 77 K, U = 2.6-3.0 V, I = 30 pA, 100 x 100 nm^2), (c) HAT+HATCN (T = 77 K, U = -1.5 V, I = 50 pA, 50 x 50 nm^2).

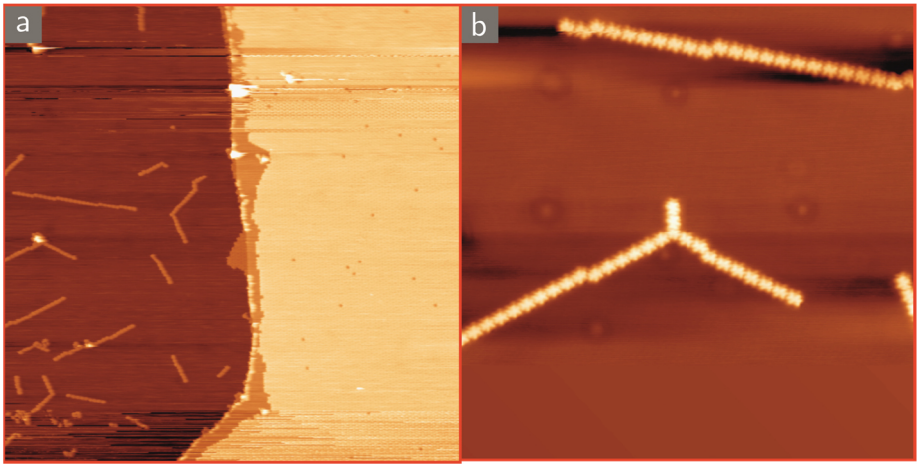

Fig. A6.3: HAT on Ag(111) showing linear chains besides a close packed island, which is visible in the right part of (a). (a) Overview image (T = 77 K, U = -1.0 V, I = 20 pA, 150 x 150 nm^2), (b) close-up view of two chains (T = 77 K, U = -1.6 V, I = 30 pA, 40 x 40 nm^2).

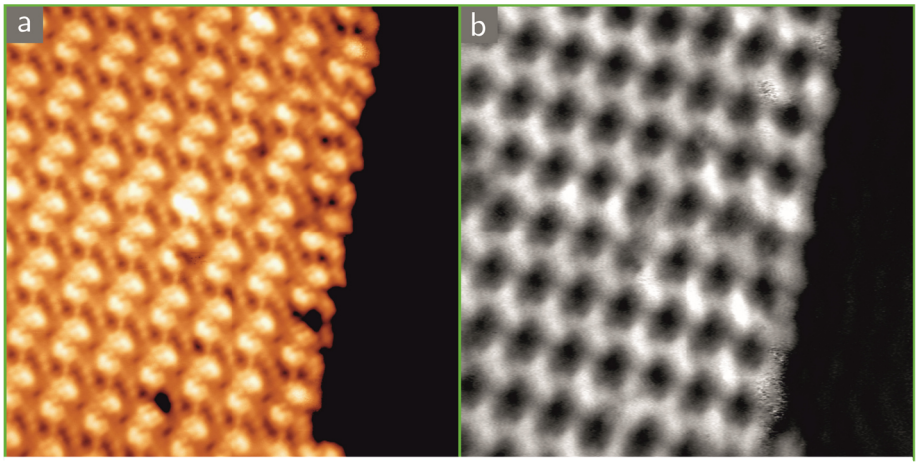

Fig. A6.4: Intermixed molecular layer: STM image (a) and simultaneously taken dI/dV map (b) taken at a bias of 0.5 V and a current of 200 pA at 5 K (20 x 20 nm^2).

Fig. A6.4 shows an STM image and the simultaneously taken dI/dV map for the intermixed HAT / HATCN layer for a bias voltage close to the LUMO (0.5 V). It is visible that the conductivity of the molecules at the border of the island is the same as in the island center. Consequently, we deduce that no electron spill-out at the boarder of the molecular islands is present.

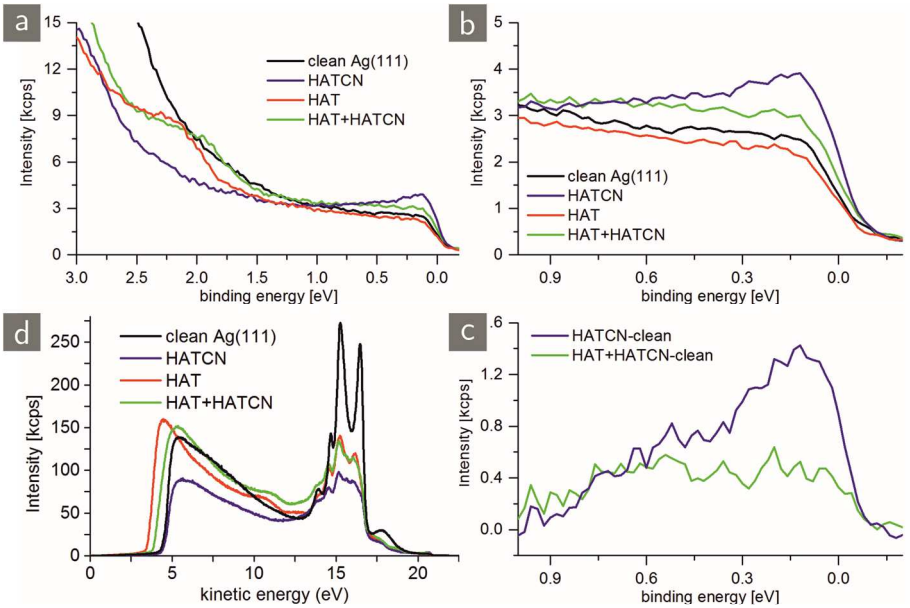

Fig. A6.5: (a), (b) UPS data for clean Ag(111) (black), and for approximately one monolayer of HATCN (blue), HAT (red) and HAT+HATCN (green). (c) Work function measurements taken with a bias of -5V applied to the sample. (d) UPS data of HATCN close to the Fermi energy after subtraction of the clean Ag(111) spectrum.

Additional Electron Spectroscopy Data

Fig. A6.5 shows angle-integrated UPS and work function measurements.

According to Goiri et al.[11] and El-Sayed et al.[21] the work function change of an intermixed molecular layer can be determined by the work function changes of the pure components as long as the surface areas occupied by the adsorbates are known:

$$\Delta_{mix} = \frac{A_{acc}}{A_{mix}}\Delta_{acc} + \frac{A_{don}}{A_{mix}}\Delta_{don} \quad (1)$$

A_{acc}, A_{don} are the areas of a single molecule in the homomolecular layers taken form the unit cells of the homomolecular layers, which are given in Table A6.1 while A_{mix} is the area for a donor or acceptor molecule in the intermixed layer. Goiri at al. used $A_{mix} = A_{acc} + A_{don}$. However, this is not possible in our case since the HATCN molecules formed a porous structure in the homomolecular layer while the bilayer formed a close packed structure. We estimated A_{mix} by using the unit cell area of the intermixed structure and dividing it by two accounting for the fact that two HAT and two HATCN molecules are present in the unit cell, and both molecules had almost the same size and occupied similar positions in the unit cells (Fig. 6.2c). This led to a theoretical work function change of -0.43 eV, which is very close to the measured value of -0.4 eV.

Table A6.1: Values for the calculation for the work function shift according to Goiri et al. (* the first value is the measured work function shift, the second one is the calculated work function shift according to equation (1); ** this value is derived from the intermixed structure unit cell assuming that the areas occupied by HAT and HATCN are similar).

	unit cell	unit cell area [nm^2]	molecules per unit cell	surface area per donor /acceptor molecule [nm^2]	work function change Δ
HATCN	2.02 x 2.02 nm^2 $\theta = 60$	3.52	2	1.76	0.0
HAT	1.32 x 1.32 nm^2 $\theta = 60°$	1.51	1	1.51	0.9
HAT+HATCN	2.4 x 2.7 nm^2 $\Theta = 77°$	6.31	2	3.16**	0.4-0.43*

The ARPES data shown in Fig. 6.4b and c in the main text where fitted with a Lorentzian function after subtraction of a linear background around the HOMO feature according to equation (2), where w equals the half-width and a_1, a_2, a_3 and x_0 are constants.

$$f(x) = a_1 + a_2 x + \frac{a_3 w^2}{(x - x_0)^2 + w^2} \qquad (2)$$

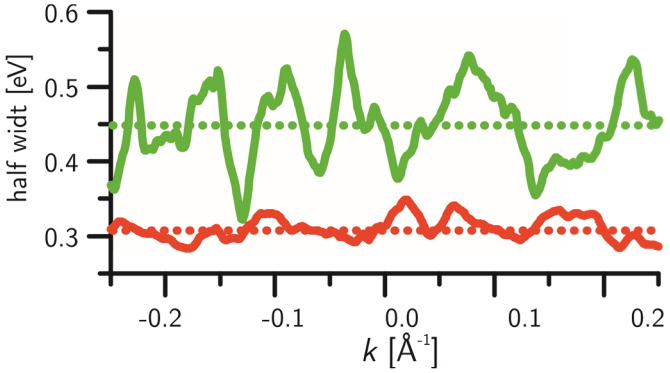

Fig. A6.6: Half-width of the HOMO of pure HAT (red) and the mixed phase (green) derived from a Lorentzian fit. The dotted lines indicate the average half-width.

The half-width for HAT and the intermixed layer are displayed in Fig. A6.6. It is clearly visible that the width of the HOMO of the homomolecular HAT is smaller than the one of the mixed layer.

Table A6.2 summarizes the binding energies and the full-width half maximum (FWHM) of the N 1s and O 1s components. It is clearly visible that the O 1s peak of HAT shifted towards lower binding energy in the intermixed structure, while the N 1s peak positions of HATCN were practically not altered upon mixing with the HAT molecules. The N 1s FWHM significantly decreased upon co-adsorption with the HAT molecules indicating a reduced interaction in the intermixed layer. In contrast, the FWHM of the O 1s peak did almost not change upon mixing of the two molecules. Figure S7 shows the C 1s spectra acquired for HAT, HATCN and the intermixed layer.

Table A6.2: XPS fitting parameters for N 1s and O 1s

	N 1s				O 1s	
	C≡N		C-N=C		C-O-C	
	E_{bind} [eV]	FWHM [eV]	E_{bind} [eV]	FWHM [eV]	E_{bind} [eV]	FWHM [eV]
HAT	N/A	N/A	N/A	N/A	533.5	1.02
HAT+HATCN	398.4	1.19	399.8	1.67	533.1	0.98
HATCN	398.5	1.46	399.8	1.75	N/A	N/A

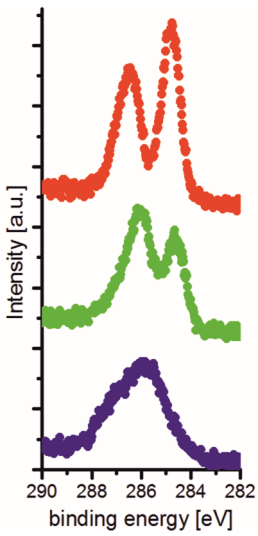

Fig. A6.7: C 1s XPS data taken for monolayers of HAT (red), HAT+HATCN (green) and HATCN (blue).

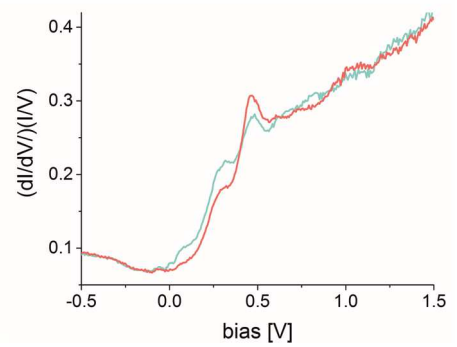

Fig. A6.8: STS data for the intermixed layer for the HATCN (light blue and the HAT (light red).

Calculated Superstructures, STM Images and DOS

For the adsorption of HATCN on Ag(111), two molecules were used per unit cell in the (7x7) supercell according to the unit cell determined by LEED (Fig. 6.2a in the main text). The center-to-center distance between two neighboring molecules was found to be 12.1 Å. The molecules occupied alternatingly 3-fold fcc and hcp hollow sites (Fig. A6.9a and b). The binding energy for this structure was found to be 2.41 eV/molecule. In Table S3, some of the geometrical details are summarized. Note that for the case of HATCN, the buckling was substantial as compared to that for HAT (Table S4). For the C-atoms, the buckling was about 0.4 Å, while that for N was about 0.65 Å. The large difference in height for the N-atoms comes from the fact that the cyano-groups bound strongly to the substrate and made the molecule bend. As a result, the otherwise flat molecule in the gas phase was arched when adsorbed on the substrate. Additionally, we also found a stronger buckling in the first silver layer, which indicates a stronger molecule/substrate interaction.

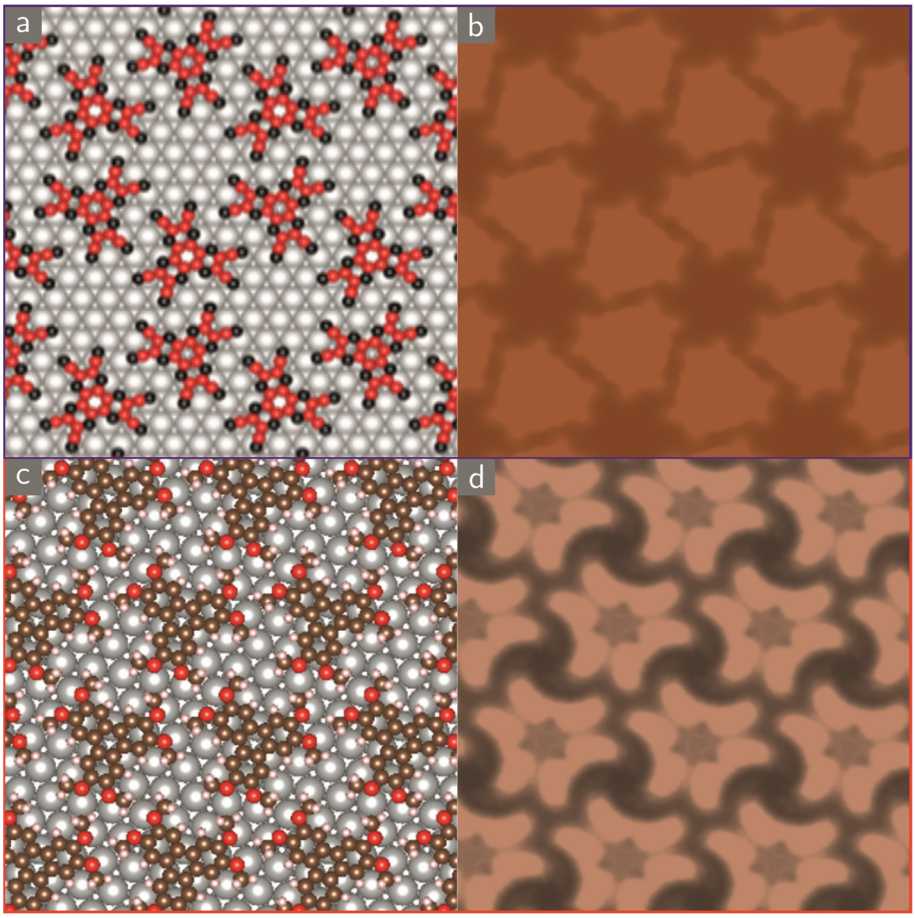

Fig. A6.9: Calculated superstructures and STM images of HATCN (a, b) and HAT (c, d) on Ag(111).

The adsorption of HAT on Ag(111) formed a ($\sqrt{21}$x$\sqrt{21}$)R10.9° superstructure as observed by LEED (Fig. 6.2b main text) . We performed calculations with the same super cell and observed that the center of the molecule lied on top of a three-fold hollow site, with a distance between two neighboring molecules (center to center) of 13.4 Å (Fig. A6.9c and d). The binding energy of a HAT molecule for this superstructure was found

Table A6.3: Geometrical details for HATCN on Ag(111).

atoms	Z-average (Å)	lowest Z (Å)	highest Z (Å)
C	19.36 (3.37)	18.97	19.17
N	18.98 (2.99)	18.65	19.31
Ag 1st layer	15.99	15.92	16.06

to be 2.27 eV. In Table S4 we summarize some of the structural information for HAT on Ag(111). While in the gas phase all atoms rested on the same plane, adsorption on the metal substrate resulted in a slight buckling in the z-plane containing the C atoms of about 0.28 Å. For the substrate, the surface atoms positions were not affected by the presence of the molecule.

From the above mentioned superstructures we also derived the electronic structures of the molecules on the Ag(111) surface. HATCN interacted much stronger with Ag(111) which resulted in a charge transfer of 2.3 electrons/molecule from the substrate. This is in line with our findings of the partially occupied LUMO, which we found in ARPES, UPS and STS. In contrast, HAT did not undergo any significant electronic

Table A6.4: Geometrical details for HAT on Ag(111).

atoms	Z-average (Å)	lowest Z (Å)	highest Z (Å)
C	19.32	19.24	19.52
N	19.36	19.34	19.41
Ag 1st layer	15.98	15.96	15.99

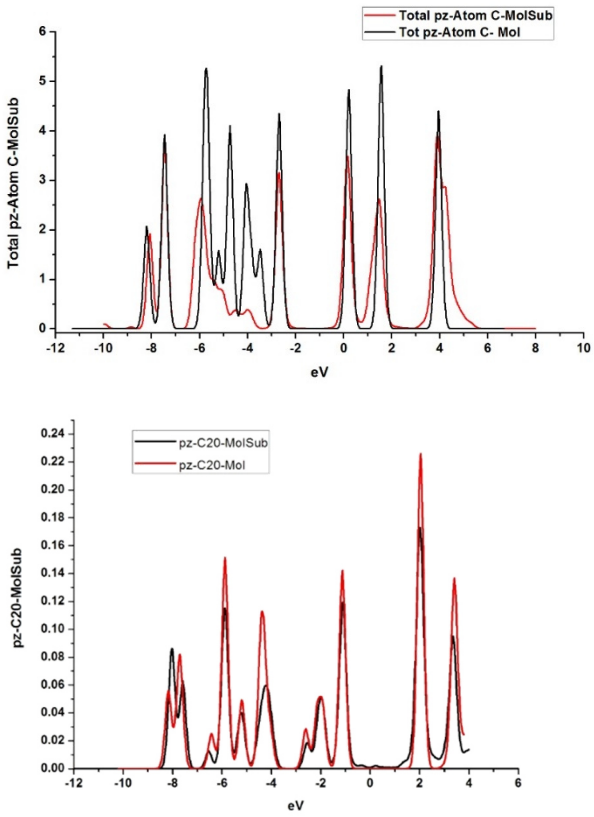

Fig. A6.10: Top: total density of the pz-states of the carbon atom for HATCN on Ag(111) and for the gas phase; Bottom: DOS of HAT on Ag(111) and for the gas phase molecules.

changes and we only found a very small charge transfer of 0.2 electrons/molecules from the substrate to the molecule. Figure S10 summarizes the calculated density of states (DOS) for the homomolecular HATCN and HAT layers on Ag(111) as well as for the gas phase molecules.